RESERVOIR CHARACTERIZATION BY AVO ANALYSIS: A CASE STUDY OF PENYU BASIN, MALAYSIA

Leam Jia Yi, Abdul Halim Abdul Latiff, Maman Hermana

Department of Geosciences, Universiti Teknologi PETRONAS, Malaysia

*Email: abdulhalim.alatiff@utp.edu.my

ABSTRACT

Amplitude variations with offset (AVO) method are applied in predicting hydrocarbon by interpreting the anomalies in terms of lithology and pore fluids using the AVO cross-plot of intercept, A, and gradient, B. The study was carried out and tested in the previously problematic field such as thick sand with non-commercial discovery in Penyu Basin, Malaysia. With limited prospect evaluation conducted in this basin, we aim to provide evidence of potential hydrocarbon accumulation exists in this region for further exploration development. The AVO response of the anomalies detected first executed in locating the potential hydrocarbon prospect before predicting shear wave velocity using the Greenberg-Castagna and Castagna equations. A statistical wavelet was then correlated with seismic data to optimize the depth-time conversion for synthetic derivation prior to fluid replacement modelling and Gassmann's equations. It is concluded that the AVO class II anomalies on both seismic and synthetic seismogram generated by AVO modelling agreed on the presence of oil in the reservoir. The AVO and seismic attributes suggested that there are potential hydrocarbon prospects in the Penyu basin based on the interpretation of structural traps of faulted anticline and fault.

Keywords: amplitude versus offset; hydrocarbon prediction; Penyu basin

INTRODUCTION

Reservoir characterization is the crucial aspect in the exploration and production (E&P) stage that utilizes all the reservoir elements – natural heterogeneity, spatial variability of permeability and porosity, porous media properties and spatial distribution of oil and water – associated with the ability to store and produce hydrocarbon. The popularity of reservoir characterization has bloomed throughout the years due to its ability in controlling the reservoir performance, development strategies and generating profit. In this work, a field located in Penyu Basin as there are less information and discovery recorded in the area. Penyu Basin is located at offshore 50 km west of Peninsula Malaysia and 40 km south of the Malay Basin. With a width of 100km and the 200km length extends westward under the Pahang river delta. The basin is divided into syn-rift and post-rift sequences and consists of mostly siliciclastic sediments aged Oligocene to recent.

A total of eight wells were drilled in the Penyu basin since the mid-60s and early 70s. Two wildcat wells, namely Penyu-I and Pari-I, initiated by the Continental Oil Company (Conoco), were unsuccessful due to the absence of hydrocarbons and poor development of the reservoir. In late 1991, once again, Texaco had made the unsuccessful discovery on the Cherating-I, Merching-I, and Rhumbia-I. It is believed that the formation of trap post-dated the oil generation window. However, the only successful discovery was in Rhu field in the year 1991, which represents a drape play over late syn-rift basement high. Due to its uneconomical investment, most of the blocks explored in the Penyu Basin were deemed as a lack of economic prospects. Hence, this study aims to determine the lateral distribution of hydrocarbon accumulation within the basin via AVO analysis to locate potential prospects for further development. AVO modelling was conducted to generate synthetic seismograms for different wells' conditions before evaluating the class of AVO response of the anomalies in the Penyu Basin.

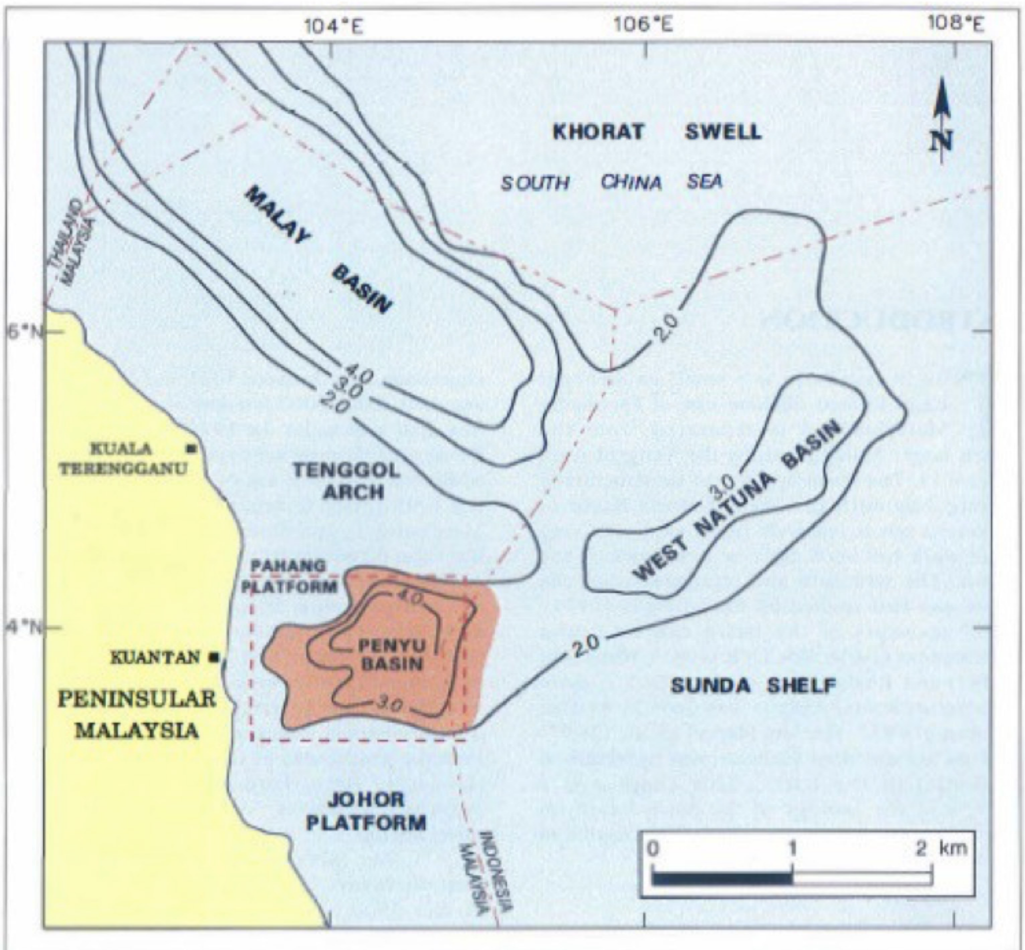

Figure 1 Location of Sunda Shelf basins-Penyu, Malay and West Natuna Basins offshore east of Peninsular [5]

the northern region is formed due to the India-Asia collision dated in the Cenozoic era. It is believed that Sundaland is generally stable in terms of tectonic activity except for the several-meters uplift that took place in onshore Johor [2]. Covering from Kota Bharu to Johor Platform in the south, three tertiary basins known as the Malay, Penyu and West Natuna basins were formed in the northern Sunda Shelf when the crest broke into three rift arms (Figure 1). The crest was due to the arch of the hot spot to the continental crust during Upper Cretaceous. As the hot spot activity ceased, these rift arms failed to result in the sedimentation of the basins [3]. The Tenggol Arch is located between the smaller extensional Penyu Basin and Malay Basin. Although the Malay and West

BACKGROUND STUDY

As the continental core of Southeast Asia, Sundaland is made up of early Tertiary basement rocks of the Sunda shelf as well as the Peninsular Malaysia and the west of Borneo. It is surrounded by converging zones in the west, south and east directions whereas, and

Natuna basins are known to have producing fields, prospects have also been identified in the Penyu basin.

The structure and stratigraphy of the Penyu basin are shown in Figure 2 [2],[4]. With a width of 100 km and 200km length extends westward under the Pahang River delta. According to Madon and Watts [5], the mild inversion that took place in Upper Miocene created broad anticlines and faults which are overlain by roughly less than a one-kilometer thickness of basin sediments. Consisting of mostly siliciclastic sediments dated to be from Oligocene to recent, the sedimentary succession of the Penyu basin is classified into syn-rift sequence formed during the extension of the basin, and post-rift structures which were formed later [4]. The Oligocene aged syn-rift sequence is made up of alluvium and lacustrine deposits whereas, the truncation and folding above the syn-rift sequence is called the Base-Pari unconformity. Coals are known to be dominant in the Pari Formation.

The petroleum system within the region is made up of lacustrine source rock, fluvial sandstone reservoir rock and shale/claystone seal. The potential source rocks are oil-prone shale made up of algal and plant organic material, Upper Eocene to Lower Oligocene age, deposited in the lacustrine environment within the half grabens [4]. The trend of Vitrinite Reflectance (VR) shows the current maturity for oil below 3000m. However, there is also the presence of poor quality gas-prone source rocks in the Penyu, Terengganu, and Pari formations. Some of the potential reservoirs of the syn-rift and post-rift structures include channel, amalgamated channel and point bar sands of coastal plain alluvial conditions whereas, good quality reservoirs are identified at the upper Penyu Formation.

The previous and only successful discovery in basin, Rhu field, represents a drape play over late syn-rift basement high. During migration, hydrocarbon travelled from the source rocks in the half-graben up the gently dipped ramp margin, to an anticline trap created by late syn-rift sediments drape over a

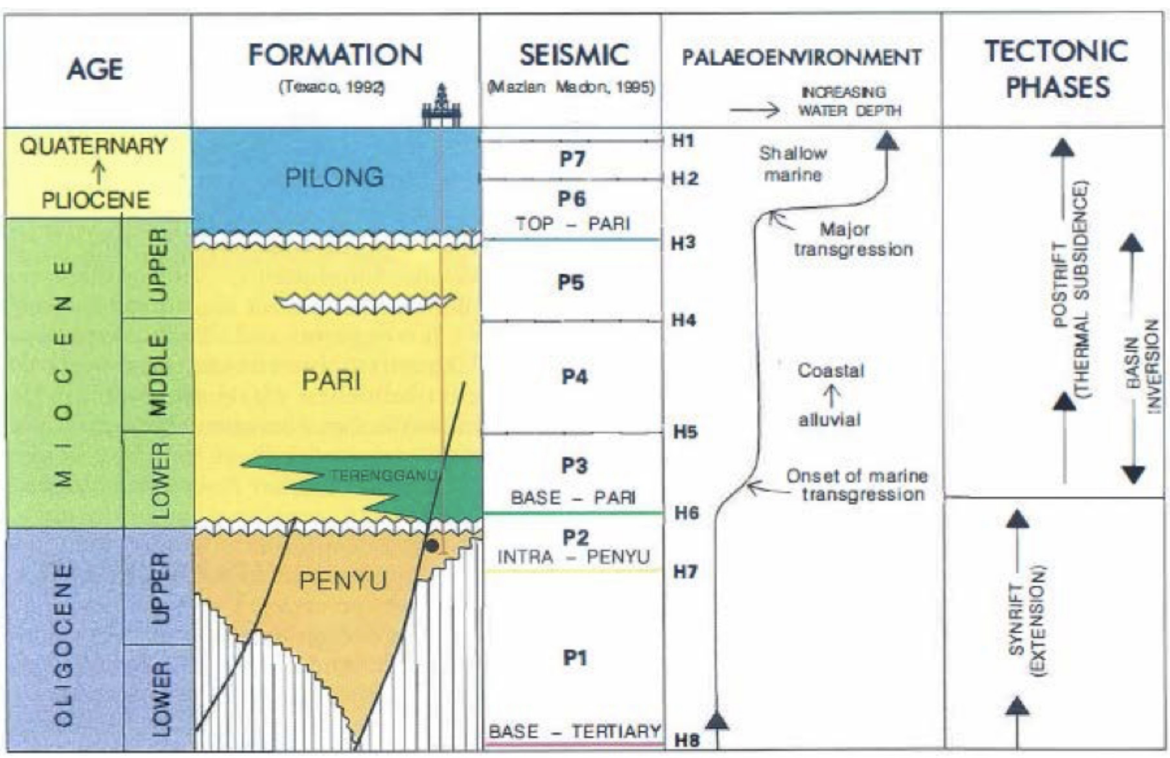

Figure 2 Stratigraphic subdivision of the Penyu Basin consisting of the syn-rift and post-rift sequences. Formation names follow Texaco's (1992) nomenclature. Seismic units, Pl to P7 are identified by markers Hl to H8 [5]

ridge in the basement. The sediment drape and fault traps overlying the ridge have been formed before migration. Thus, bed-parallel migration instead of vertical migration via fault passage is the main focus of this trap structure [4]. Figure 3 shows the petroleum system of Rhu field.

as a direct hydrocarbon indicator (DHI) [6]. This has further bloomed the technique of AVO as not only a "seismic lithology" tool but also in providing a better model for normal incidence reflection coefficients and "background" velocities prediction, with the ultimate goal of identifying new prospects.

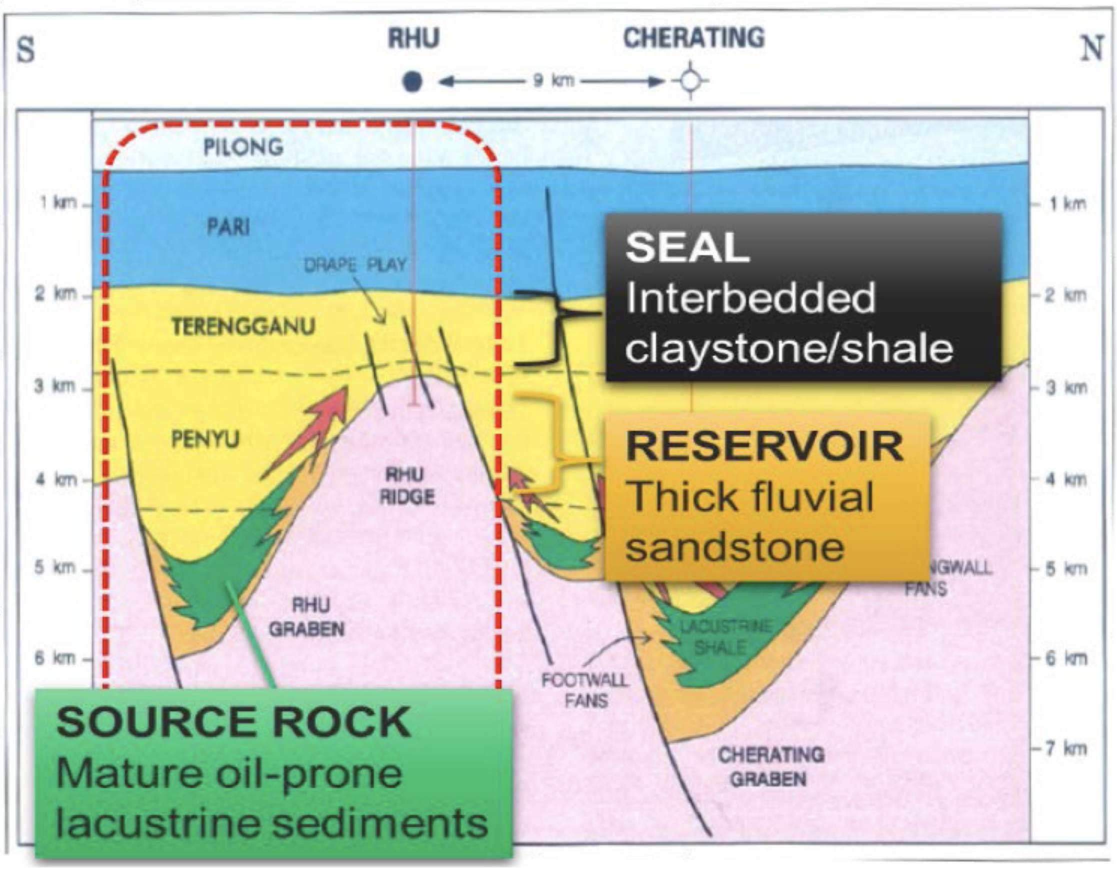

Figure 3 Petroleum System of Rhu field showing Penyu Formation as the reservoir in a drape play over late syn-rift basement high [5]

In this study, reservoir characterization is done by integrating the geophysics, petrophysics and geology data by utilizing the Amplitude variations with offset (AVO) method. Traditionally, seismic signals have been interpreted as a series of band-limited normal incidence reflection coefficient that shows the appropriate variation in terms of travel time and amplitude as they travel deeper into the subsurface. However, in 1982, it was concluded that there is an anomaly in the gas sand reflection coefficient as offset increases, thus proving this anomalous manner

AVO analysis can interpret anomalies in terms of lithology and pore fluids by using the AVO cross-plot of intercept, *A*, and gradient, *B*, [7]. Under normal conditions, the *A* and *B* for brine-saturated sandstones and shales show an appropriate "background" trend. Any variations from this background are described as "AVO anomalies" and are often associated with hydrocarbon. Zoeppritz's equations investigate the relationship between transmitted, reflected and refracted P and S-wave to determine the propagation of each ideal plane wave. Shuey's approximation [7] to

Zoeppritz equations can be defined as a function of AVO intercept, *A*, and gradient, *B*, in (1). *A* represents the normal incidence, whereas, *B* measures the amplitude variations with offset.

$$R_p = A + B \sin^2\theta + \dots \quad (1)$$

R_P: reflection coefficient θ: angle of incidence
A: AVO intercept B: AVO gradient

The AVO responses are categorized into three classes [8] whereas, Class IV was introduced in 1997 [7]. These categories are compiled and compared in Figures 4a and 4b. Class I is defined as a positive impedance contrast with a negative AVO gradient. Thus, the positive reflection coefficient decreases with offset. Next, class II is shown as small incidence reflection coefficients, regardless of the reflectivity, and has a negative gradient which leads to high reflection coefficients at far offsets. Besides, class III exhibits a high contrast of negative impedance with a negative gradient, resulting in an increase in amplitude as angle increases. On the other hand, class IV response shows a large negative normal incident reflection coefficient with decreasing amplitude as offset increases.

Through Fluid Replacement Modelling (FRM) and Gassmann's equation on reservoir well data, AVO behaviour in each reservoir condition in terms of changes in fluid type and saturation can be studied. FRM is defined as the alteration of fluid type and its saturation at the reservoir before generating synthetic logs of each scenario created [8]. Often, only one well data is acquired in a well with in-situ fluid saturation conditions. In such a situation, it is impossible to model the AVO response for different types of reservoir conditions. As a solution, the reservoir rock with existing fluids (in-situ condition) shall be modelled prior to the prediction of synthetic logs by replacing the fluid types and saturation. With the P-wave, S-wave and density logs as input, Bakhtiari, Farahbakhsh, and Moghadam [8] suggested utilizing Zoepprtiz's equations to create synthetic seismogram. The AVO behaviour on the reservoir with different pore fluid scenarios can be monitored by comparing seismic data with the synthetic seismograph generated. The modelling of reservoir rock is computed using Gassmann [9]. Computation of Gassmann equations is done to estimate the alteration of seismic properties at the reservoir such as density, compressional and shear wave velocity, caused by the fluid substitution.

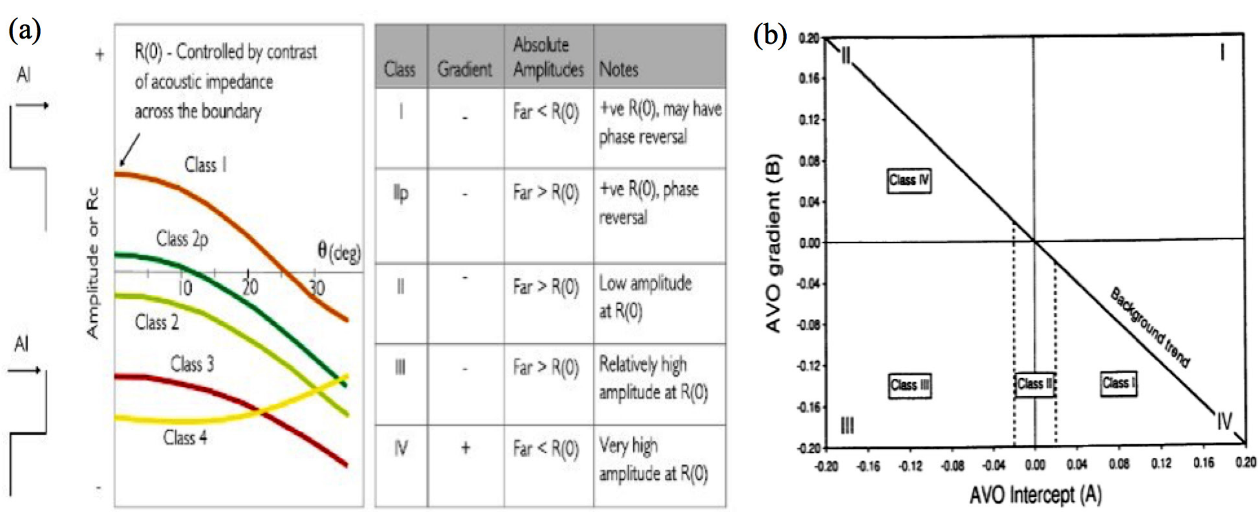

Figure 4 (a) AVO responses categorized in Classs I, II, III and IV [1],
(b) AVO classes based on AVO cross-plot

METHODOLOGY

The regional geology of the project area is studied and revised to establish a better understanding of identifying the core problem that needs to be solved in this project. Adequate knowledge in tectonic evolution, stratigraphy, sedimentary and depositional environment as well as the petroleum system on the oil field is the key focus in the geological study to produce accurate interpretation and results.

horizon picking. The horizon is then picked on a larger post-stack vintage data before importing into the Hampson-Russell software as the top of the reservoir for the pre-stack seismic data. AVO Modelling is conducted using Fluid Replacement Modelling and Gassman's Equations to model the reservoir rock from existing conditions (in-situ) to pure gas, pure oil, and pure brine scenarios. The Zoeppritz's equations are then utilized to create a synthetic seismogram for each scenario after a good well correlation is obtained.

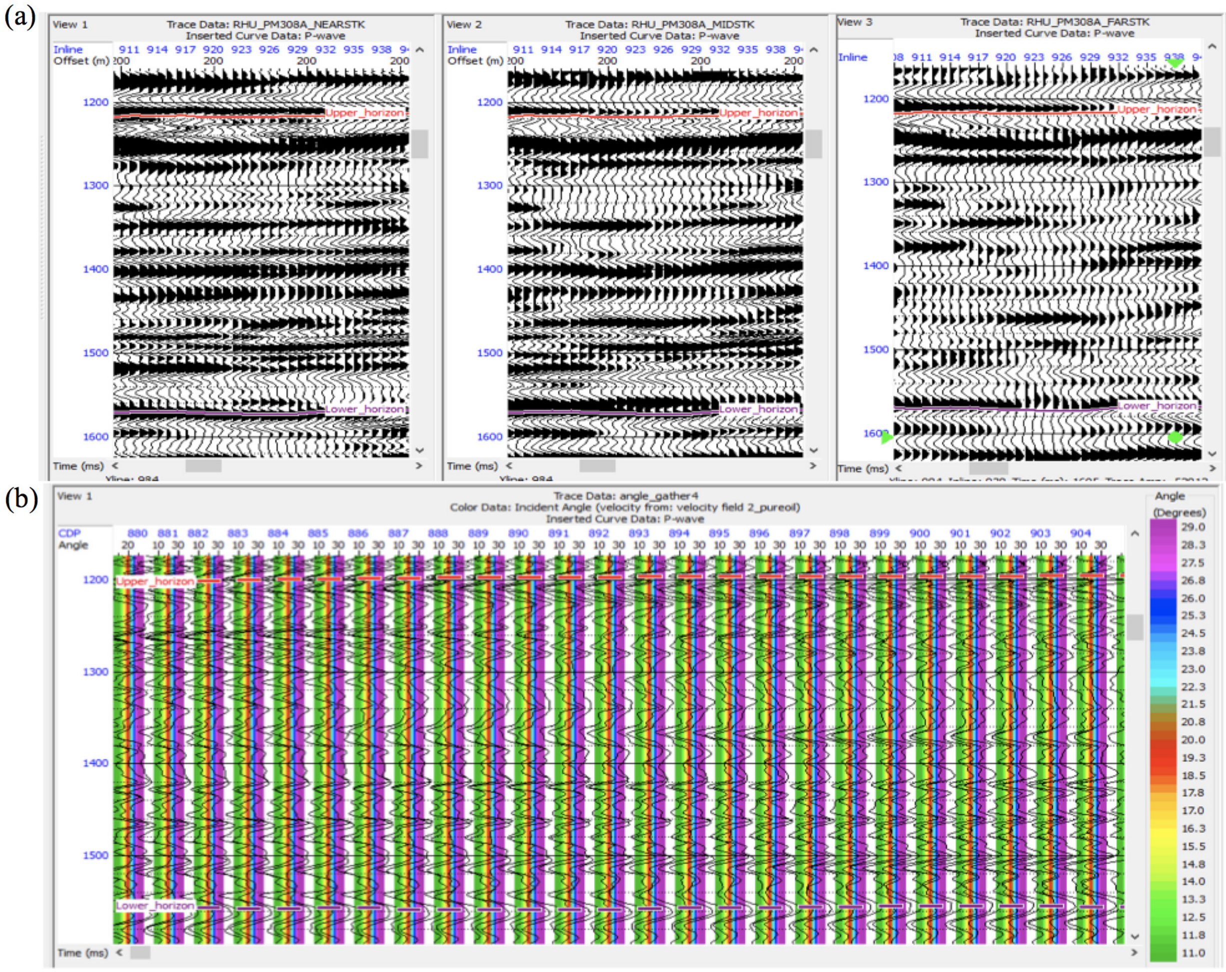

Figure 5 (a) Seismic volumes showing Near, Mid and Far angle stacks from left to right before generating angle gathers. (b) Seismic stack sections consisting of near (5°-15°), mid (15°-25°) and far angles (25°-35°) are combined to generate angle gather of 10°,20° and 30°.

This project consists of two types of data, namely the well and seismic data. One of the data limitations encountered is the Rhu-1 well, located out of the pre-stack seismic data range. As a solution, the well data is interpreted to identify the zone of interest for

A series of data pre-conditioning is conducted on the seismic pre-stack data, which includes the generation of angle gather from the near, mid and far angle volumes (Figure 5a and 5b) and the implementation of trim statics to obtain flatter events

(Figure 6a and 6b). The pre-conditioned seismic angle gathers, and the synthetics are used as the input for AVO Analysis to identify the class of anomalies from the AVO cross-plot. The results are then interpreted to locate potential hydrocarbon prospect(s) in the Penyu basin. An attribute slice of the top of the reservoir is also produced to analyze the location of prospect(s). Lastly, the results are interpreted using a multi-attribute approach, in which AVO and seismic attributes are utilized to provide more evidence for the potential prospect. Figure 7 shows the project workflow.

AVO Modelling and Analysis

As the measured shear wave log is not provided, shear wave estimation is crucial for fluid replacement modelling and Gassmann's equations. Based on Figure 8, the top and base of the reservoir are picked based on the interpretation of well log and proven oil show in the well reports. The reservoir exhibits a drop in Gamma-Ray values for approximately 20m thickness, which is also shown in the low shale volume in Vshale (shale volume) log.

(a)

(b)

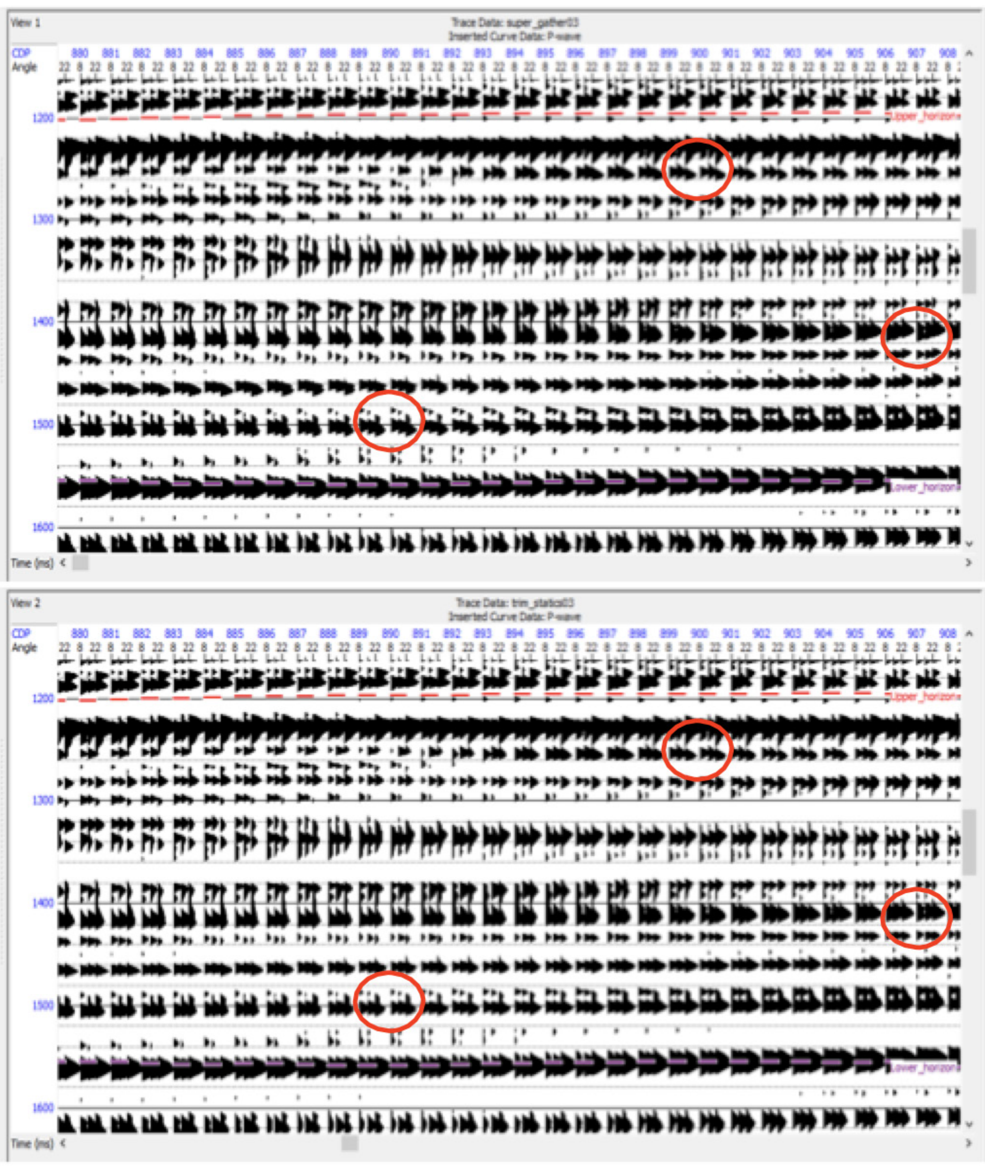

Figure 6 (a) Angle Gathers before trim statics. Red circles show the unaligned events which could be due to unoptimized processing, (b) Angle Gathers after trim statics. Red circles show the flatter events obtained

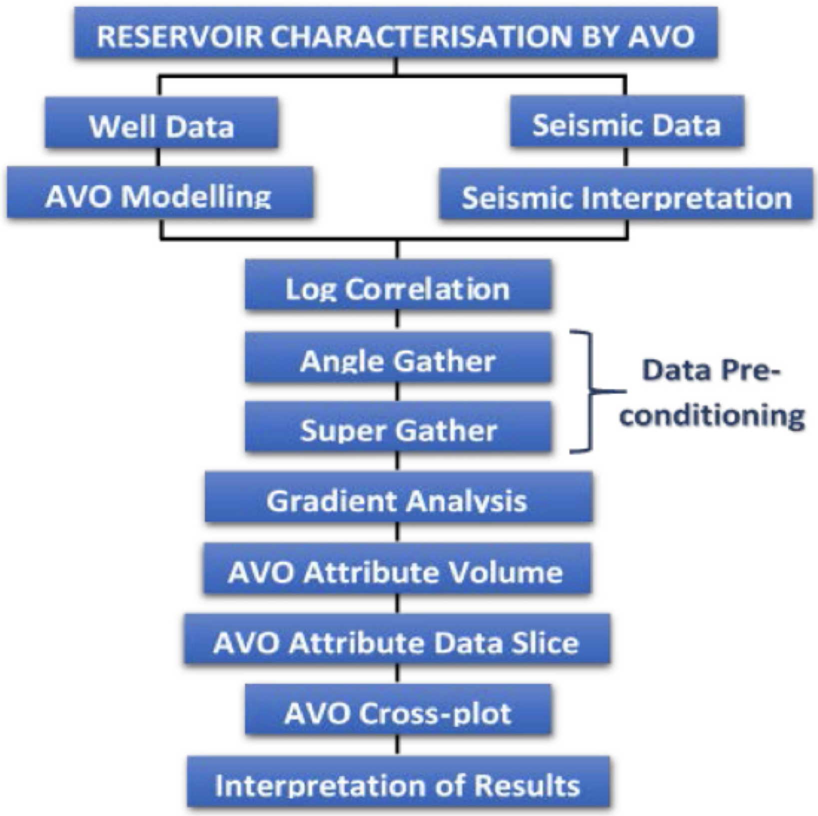

Figure 7 Project workflow

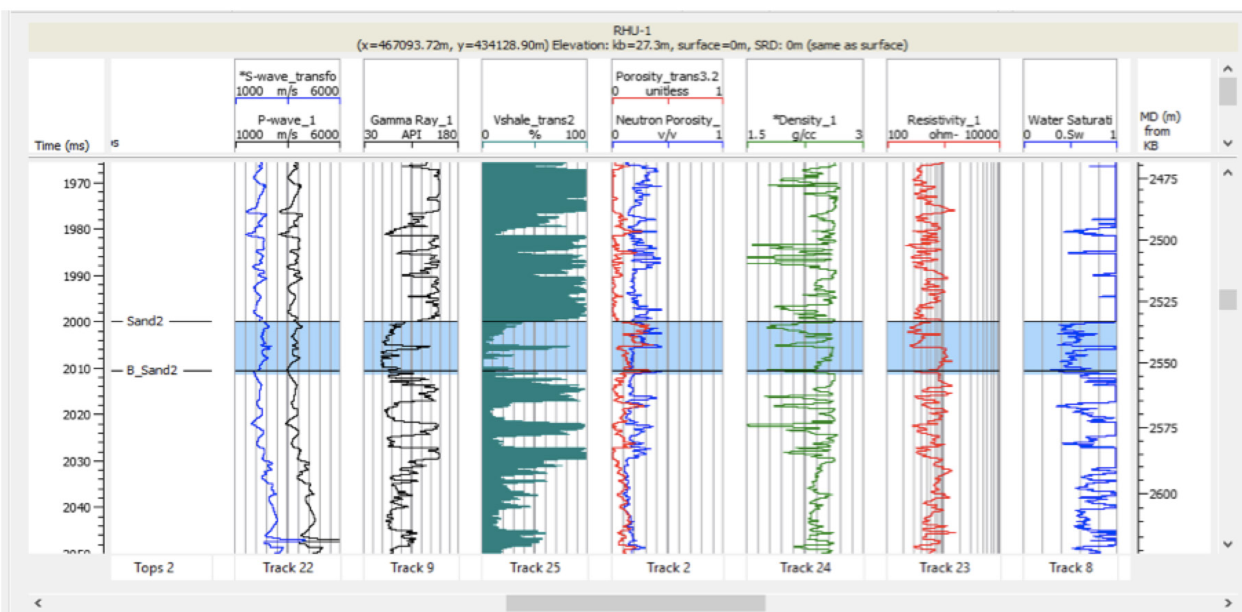

Figure 8 Well log responses at the location of interest are respectively from right to left showing P and S-wave velocities, gamma-ray, the volume of shale, porosities, bulk density, resistivity, and water saturation

Higher resistivity and porosity values of the reservoir show the presence of hydrocarbon. The low water saturation curve further proves the validity of the reservoir. From the predicted shear wave velocity log, it can be concluded that S-wave generally has a lower velocity with a similar trend as the P- wave. Figure 9 shows the wavelet extraction, which is needed for synthetics derivation by estimating the amplitude spectrum from the seismic data by assuming it to be at zero phases. A time window of 1500ms to 2700ms around the location of interest is included for wavelet extraction, and a zero-phase wavelet with a dominant frequency range from 20Hz to 60Hz is generated prior to well correlation.

Well correlation comes into play by correlating the statistical wavelet with seismic data to optimize the depth-time conversion for synthetic derivation. A maximum correlation coefficient of 0.731 (Figure 10) obtained between the statistical wavelet and seismic data at the zone of interest is sufficient. The zone of interest is located within the set cross-correlation window, which is 1970ms to 2050ms. Different scenario logs are created according to the fluid type, where a scenario is defined by the geological conditions that will be modelled with different fluid type and saturation within the reservoir. Scenarios that are modelled include the in-situ, pure gas (gas saturation at 100%), pure oil (oil saturation at 100%) as well as pure

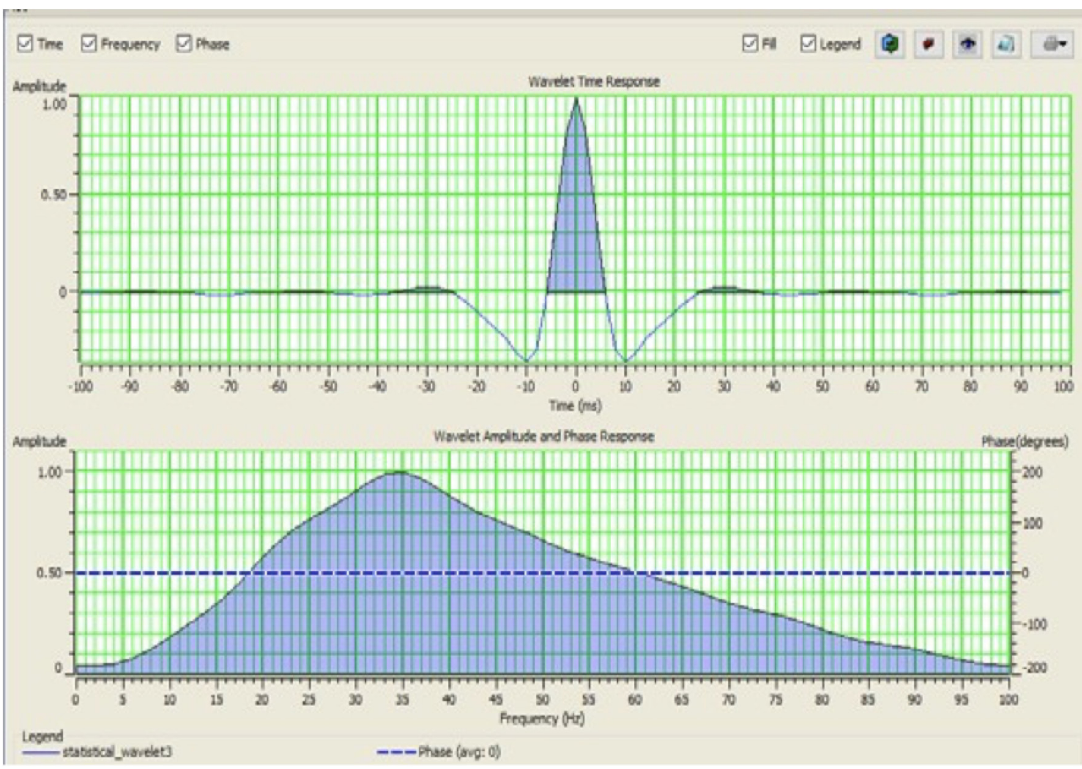

Figure 9 Statistical wavelet extraction. The time- domain wavelet is shown in the upper window, whereas, the amplitude and phase spectra are in the lower window

brine (brine saturation at 100%), as shown in Figure 11. The in-situ scenario is made up of the original fluid composition and its saturation in the well.

The log of the reservoir of pure gas exhibits the lowest density, followed by pure oil and pure brine. Due to its low-density values, S-wave log shows the highest velocity for gas and lowest for brine. This is because the shear modulus, μ, of fluid is zero. On the other hand, P-wave velocity is the highest for brine and lowest for gas even though the density of brine is higher. This is because the bulk modulus, *K*, of brine is much higher than that of gas. After obtaining the right depth-time conversion from well correlation, Zoeppritz's ray-tracing method is used to derive the synthetics from the extracted wavelet according to each scenario. Similar to the seismic pre-stack data, angle gathers ranged from 5 to 25 degrees are generated. The correlation window in Figure 12 shows that the major events in both synthetic gathers and seismic post-stack data matched, concluding that a good correlation is obtained between the synthetic seismogram and seismic data.

Aki-Richard's two-term equation is used to analyze the relationship between AVO intercept, *A*, and gradient, *B*. *A* represents the amplitude at zero offsets whereas, *B* measures the changes of amplitude with angle. Based on the cross-plot of *A* against *B* and amplitude vs angle graph from the gradient analysis in Figure 13, a background trend consisting of shales and/or brine-saturated sandstones is found to be of class I and IV that shows a decrease in amplitude with offset whereas, class II AVO anomaly response is shown where amplitude close to zero increases with the angle in pure brine (Figure 13a) and pure oil scenario (Figure 13c). However, pure oil modelling best matches the in-situ (Figure 13d) and seismic data in inline 1005 and crossline 2790 (Figure 13e). Thus, agreeing on the existence of oil in the reservoir, as stated in the well reports. The synthetics of pure gas, on the other hand, show a class III AVO anomaly response that indicates the presence of gas in the reservoir (Figure 13b).

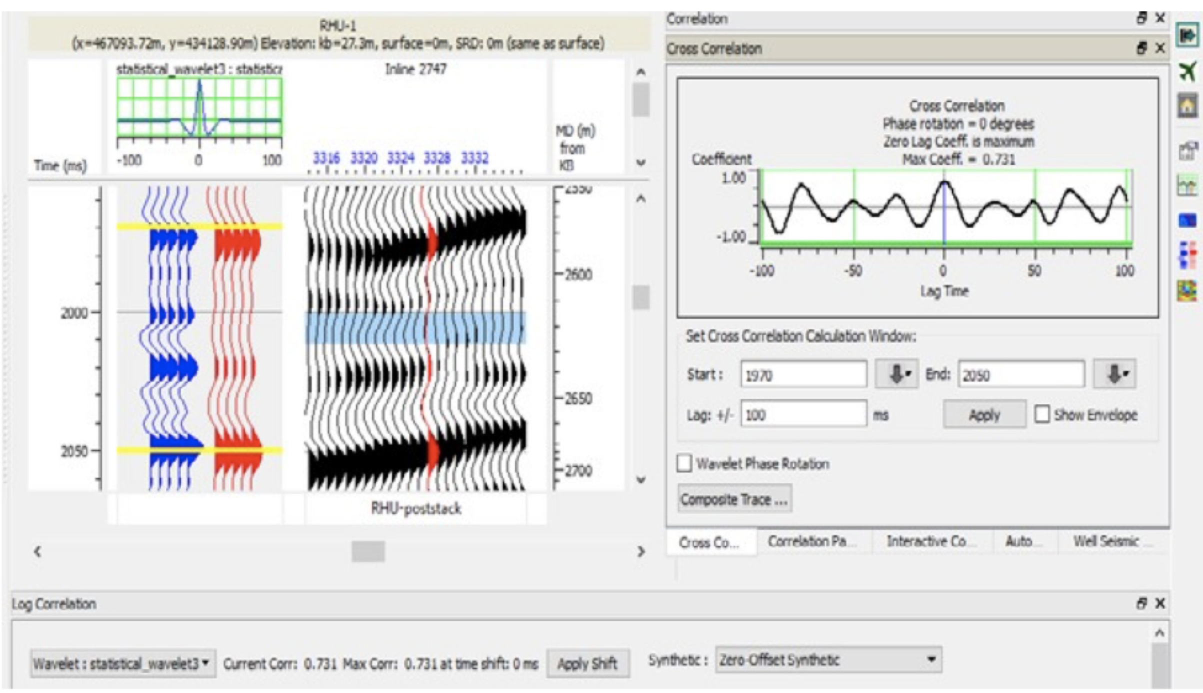

Figure 10 Well correlation window at 1970ms to 2050ms. The window at the right shows the maximum correlation coefficient of 0.731

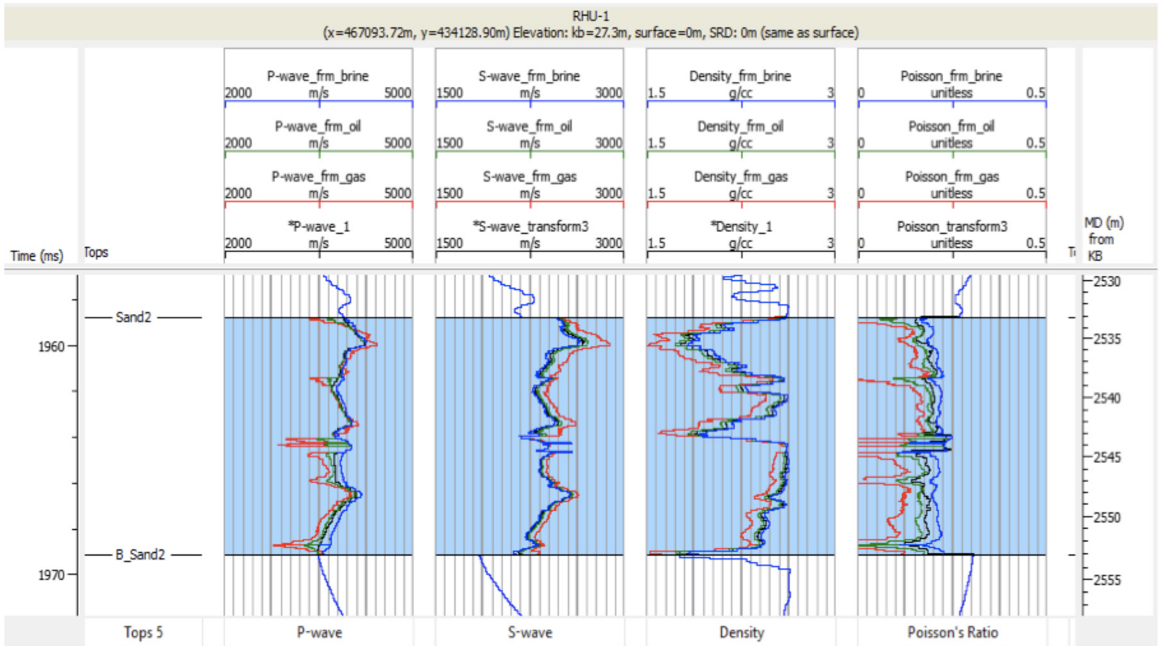

Figure 11 Synthetic logs for each scenario – in-situ, pure gas, pure oil, and pure brine – showing the P-wave and S-wave velocities, density, and Poisson's ratio respectively from left to right

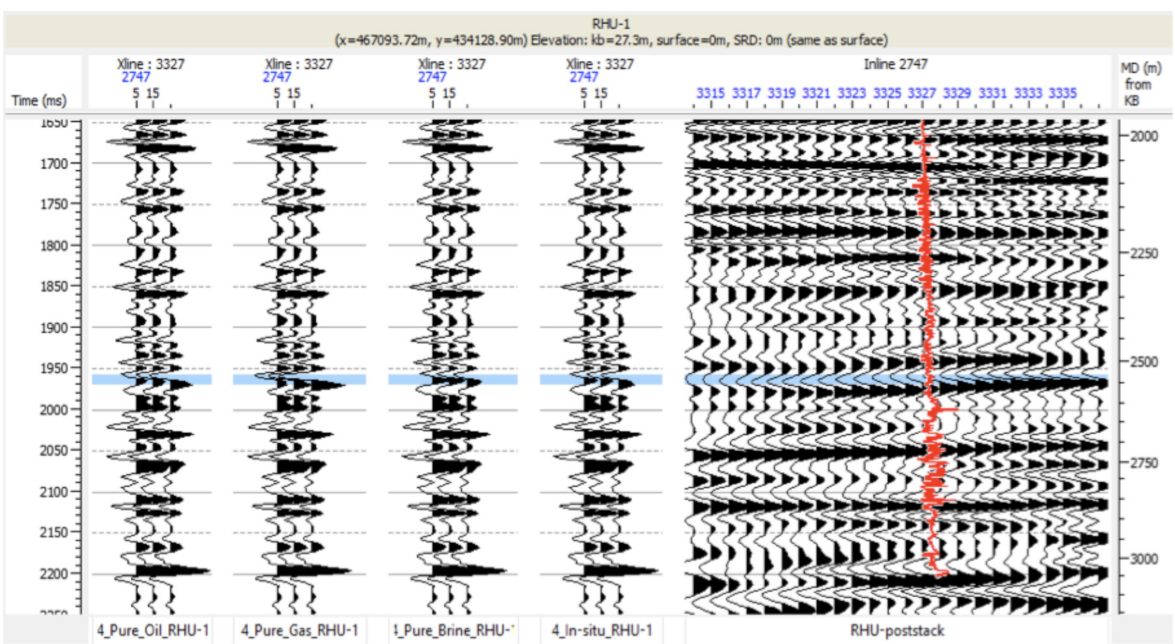

Figure 12 Correlation between the synthetics of – pure oil, pure gas, pure brine, in-situ – scenarios from left to right, respectively and seismic data at the left

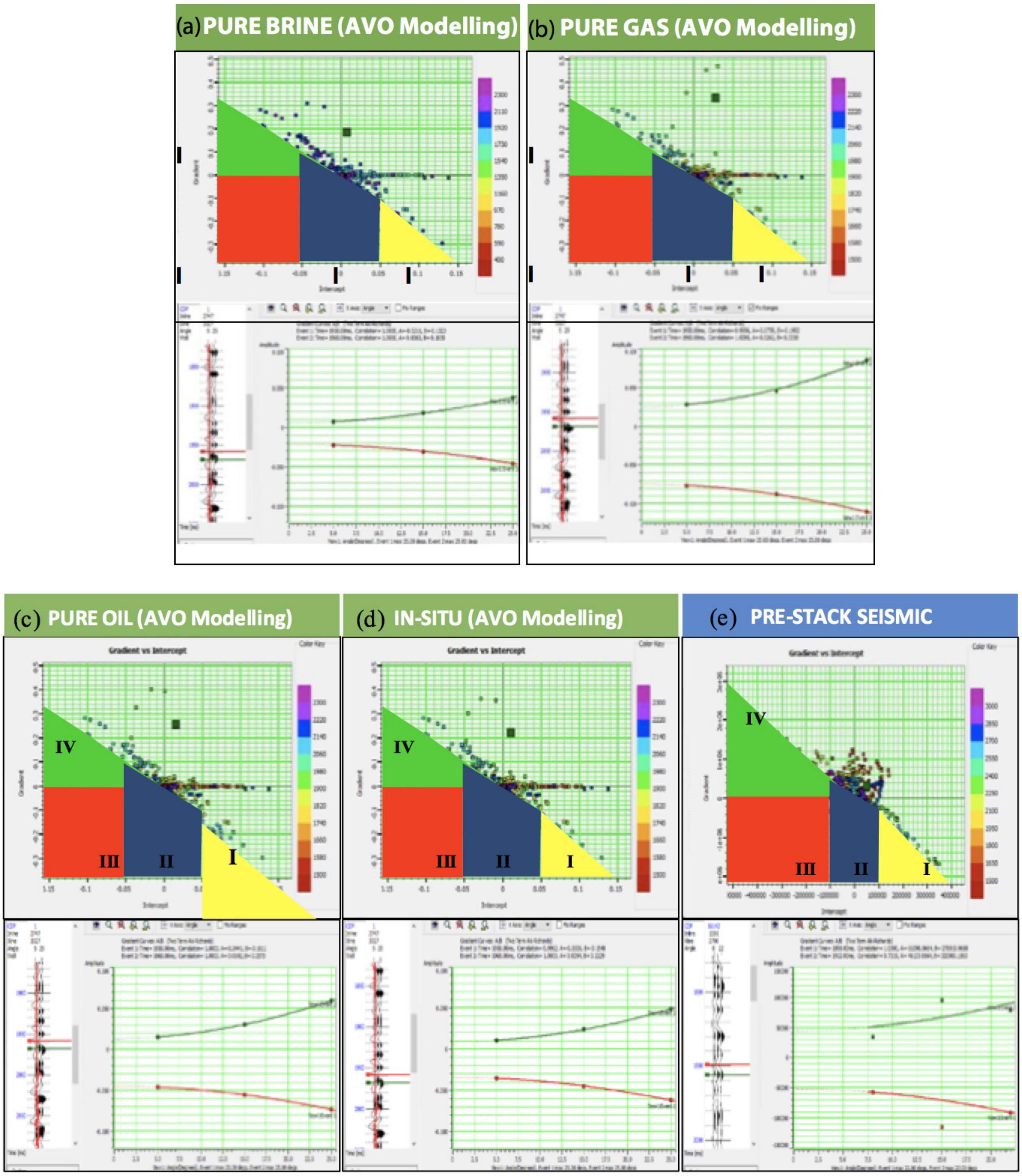

Figure 13 AVO cross-plots with reservoir top marked in red and base marked in the green of (a) Class II AVO response in pure brine synthetics where amplitude close to zero increases with angle. Anomaly is located close to the background trend, (b) Class III AVO response in pure gas synthetics where amplitude increases with angle. Anomaly is located furthest from the background trend, (c) Class II AVO response in pure oil synthetics where amplitude close to zero increases with angle. Anomaly is located slightly further from the background trend as compared to pure brine scenario, (d) Class II AVO response in in-situ synthetics matches the seismic data and shows the closest comparison with pure oil scenario, thus validates the existence of oil in the reservoir as stated in the well reports, (e) Class II AVO response on seismic data on inline 1005 and crossline 2790

Attribute Analysis

Figure 14 shows a cross-plot of intercept, *A,* against the gradient, *B,* created from the AVO Analysis on the 3D seismic data with a polygon drawn to categorize the class II AVO anomalies. The overlaying of anomalies on the seismic data is used to identify the potential hydrocarbon accumulation (Figure 15a and 15b). On the top of the reservoir where most of the anomalies are located, two potential hydrocarbon prospects are identified from the seismic sections which are structural traps of faulted anticline and fault (Figure 15c and 15d).

the sum of intercept, *A*, and gradient, *B,* and gives a rough approximation to the change in Poisson's ratio, which acts as a good indicator of fluid saturation. From Figures 16c and 16d, a negative response shown in orange or green is located at the top of reservoir indicating a drop in Poisson's ratio whereas, the base of reservoir exhibits strong positive response shown in blue or yellow indicating an increase in Poisson's ratio. The reduction in Poisson's ratio usually suggests the presence of pore fluid. In most cases, the greater the compressibility of the fluid, the lower the Poisson's ratio.

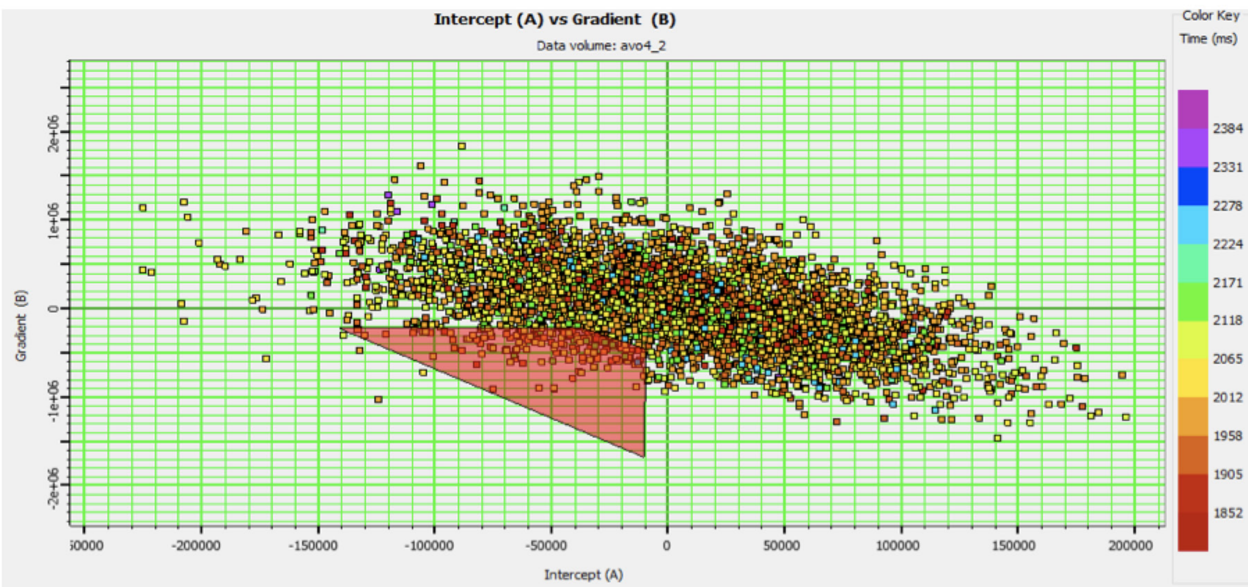

Figure 14 AVO cross-plot of 3D pre-stack seismic volume with a red polygon drawn to categorize the class II anomalies, which indicate brine

The multi-attribute approach (Figure 16) is conducted to provide more evidence on the potential of Prospects 1 and 2. The first AVO attribute used is the class II anomalies from AVO cross-plot, which are shown to be more concentrated at the top of the reservoir, suggesting the possible hydrocarbon accumulation (Figure 16a and 16b). The next AVO attribute used is the Scaled Poisson's Ratio Change created from

To crosscheck the results obtained from AVO attributes, a seismic attribute (Equation 2) generated from the seismic traces, in which *F* represents Far Stack traces and *N* represents Near Stack traces, is used to indicate the rise in amplitude with offset.

$$\text{Seismic Attribute} = (FF - NN) \times FF \quad (2)$$

As expected, Figure 16e and 16f show high amplitude at the circled area of Prospects 1 and 2, which are consistent with AVO class II behaviour. Besides, an attribute slice is also generated in Figure 17 to observe the amplitude envelope on the top of the reservoir.

An amplitude envelope is an attribute independent of phase which provides better reliability in interpretation. High amplitude observed at the highlighted areas indicates that the findings on the potential of Prospects 1 and 2 have been consistent.

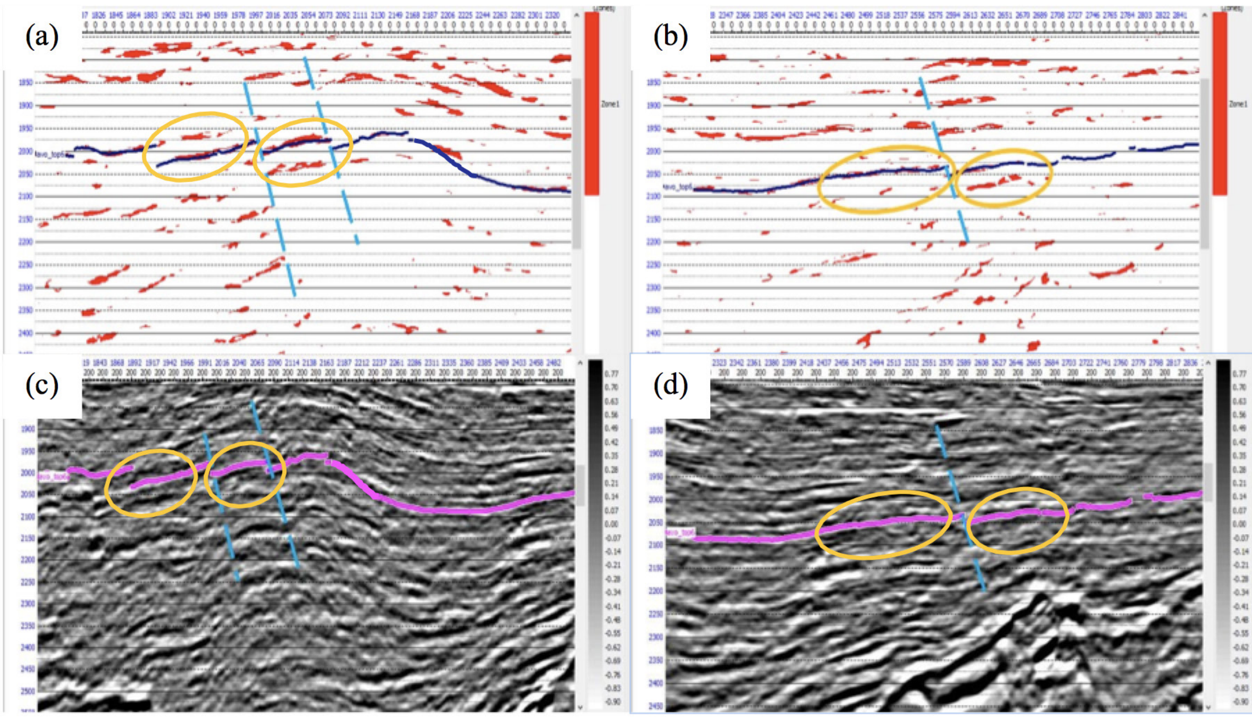

Figure 15 Overlay of anomalies on seismic data on (a) faulted anticline trap of Prospect 1 and (b) fault trap of Prospect 2. Seismic data in grayscale showing the (c) Prospect 1 and (d) Prospect 2, as highlighted in the yellow circles

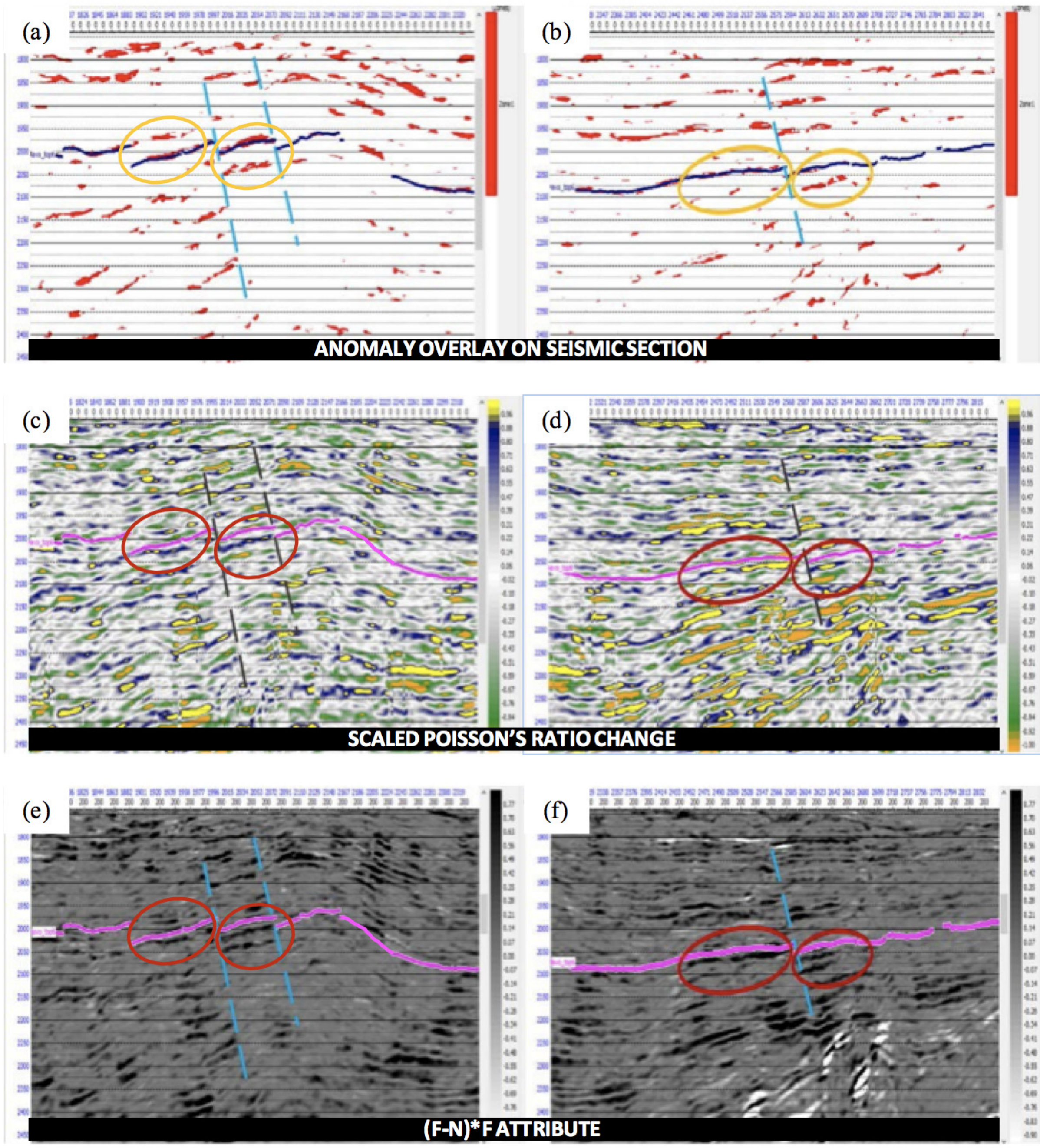

Figure 16 Anomaly overlay on seismic data for (a) Prospect 1 and (b) Prospect 2. Scaled Poisson's Ratio Change attribute on (c) Prospect 1 and (d) Prospect 2, showing a decrease in Poisson's ratio at the top of the reservoir and increase at the base of the reservoir. The seismic attribute of (F-N)*F showing high amplitudes at circled areas for (e) Prospect 1 and (f) Prospect 2

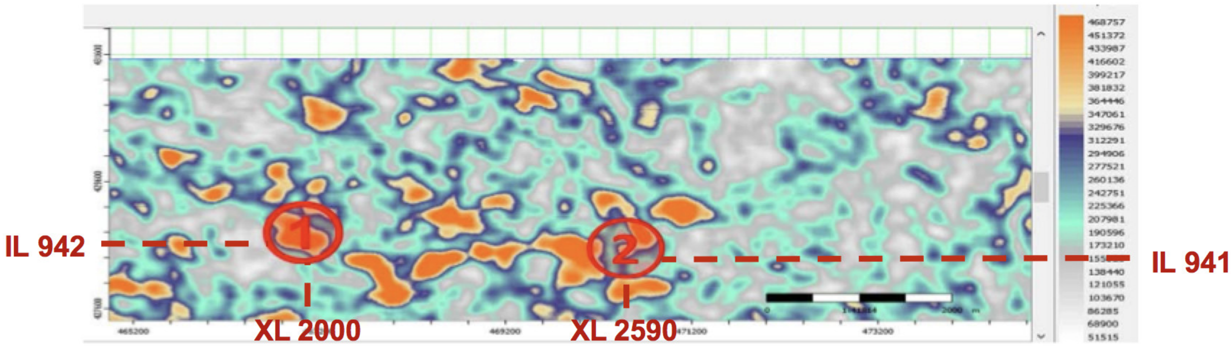

Figure 17 Attribute slice of the amplitude envelope on top of the reservoir showing high values at Prospect 1 and 2. The location of both prospects is highlighted

CONCLUSIONS

In this research, AVO Analysis is done to predict hydrocarbon accumulation in the Rhu field of Penyu Basin for further development. AVO Modelling is conducted by performing Fluid Replacement Modelling and Gassmann equations on a well data in Penyu basin, to generate synthetic logs and gathers of different scenarios. AVO Class II response of anomalies on both seismic and synthetic seismogram generated by AVO Modelling further proved the presence of oil in the reservoir within the Penyu basin region. The lateral distribution of hydrocarbon is also obtained by overlaying the class II anomalies on the seismic data, where two possible prospects are identified.

A multi-attribute approach that includes the AVO anomaly scaled Poisson's Ratio, seismic trace attribute and amplitude envelope are conducted to provide evidence for hydrocarbon accumulation. Both AVO and seismic attributes suggested that the potential hydrocarbon prospects in the Penyu basin are structural traps of the faulted anticline (inline 942, crossline 2000) and fault (inline 941, crossline 2590). In conclusion, all the objectives of this study are accomplished. It is recommended to undergo re-processing with more advanced algorithm for better imaging at the deeper areas and to perform a pre-stack inversion using the re-processed seismic data to delineate the reservoir sand by enhancing the resolution. The integration of geophysics, petrophysics, and geology knowledge in this project aim to benefit any future studies in the rarely explored Penyu Basin.

REFERENCES

[1] R. Hall and C. K. Morley, "Sunda Land basins", *Continent-Ocean Interactions Within East Asian Marginal Seas,* pp. 55-85, 2004.

[2] H. Tjia and K. Liew, "Changes in tectonic stress field in northern Sunda Shelf basins", *Geological Society, London, Special Publications,* 106, pp. 291-306, 1996.

[3] H. Tjia, "Origin and tectonic development of Malay-Penyu-West Natuna basins", *PRSS Technology Day,* 21, 1998.

[4] M. B. H. Madon., A. Anuar, "Penyu Basin", *Petroleum Geology and Resources of Malaysia* pp. 221-233, 1999.

[5] M. B. Madon and A. Watts, "Gravity anomalies, subsidence history and the tectonic evolution of the Malay and Penyu Basins (offshore Peninsular Malaysia)", *Basin Research,* 10, p. 392, 1998.

[6] J. P. Castagna and M. M. Backus, "Offset-dependent reflectivity: Theory and practice of AVO analysis", *Society of Exploration Geophysicists*, 1993.

[7] J. P. Castagna and H. W. Swan, "Principles of AVO cross plotting", *The Leading Edge,* 16, pp. 337-344, 1997.

[8] S. R. Bakhtiari, E. Farahbakhsh, and R. H. Moghadam, "Application of AVO attributes and fluid replacement in determining AVO anomaly: Case study of Aboozar oil field, Iran," *Journal of Tethys,* 2, pp. 242-253, 2014.

[9] F. Gassmann, "Elastic waves through a packing of spheres", *Geophysics,* 16, pp. 673-685,1951.